Interaction of laser generated ultrasonic waves with wedge-shaped samples

R.S. Edwards,[a] B. Dutton, and A.R. Clough

Department of Physics, University of Warwick, Coventry, CV4 7AL, UK

Wedge-shaped samples can be used as a model of acoustic interactions with samples ranging from ocean wedges, to angled defects such as rolling contact fatigue, through to thickness measurements of samples with non-parallel faces. We present work on laser generated ultrasonic waves on metal samples; one can measure the dominant Rayleigh-wave mode, but longitudinal and shear waves are also generated. We present calculations, models and measurements giving the dependence of the arrival times and amplitudes of these modes on the wedge apex angle and the separation of generation and detection points, and hence give a measure of the wedge characteristics.

PACS numbers: 43.20.Bi, 43.20.Ye, 43.40.Le, 81.70.Fy

Keywords: Laser Ultrasound, Ultrasound Modeling, Wedge, Sample Characterisation

[a]Electronic mail: r.s.edwards@warwick.ac.uk

Ultrasonic measurements have a wide range of applications in non-destructive testing (NDT), including thickness gauging[1], defect detection and characterisation[2–5], as well as in areas such as predicting the behaviour of seismic waves incident on ocean wedges[6–8]. In NDT, ultrasonic waves are often considered to propagate in half spaces or finite-thickness samples with parallel faces. However, understanding of the interaction of ultrasonic waves with more realistic geometries requires alternative samples: for example, a wedge-shaped sample can be used as a first step to model a defect propagating at an angle to the surface, as with rolling contact fatigue (RCF) in railway tracks[9], or a sample with non-parallel front and back faces.

Whilst used somewhat in geophysics to calculate propagation of seismic waves[6–8], wedge-shaped samples are just starting to be considered for modelling propagation in NDT. One dimensional wedge waves propagating in a wedge-shaped sample have been shown to have a dispersive nature, which depends on the wedge thickness at each point[10–12]. The wedge can also model an infinite depth crack which propagates at an angle to the surface[2–5,13,14]; the reflection and transmission coefficients have a dependence on the angle of the defect, and the arrival times of the transmitted wavemodes can be used to measure the crack angle[4,13,15,16]. A wedge sample has also been used to demonstrate the mode-conversion of the Rayleigh wave to a guided wavemode as the frequency·thickness product decreases, leading to a much larger signal enhancement at the defect for angled defects than for defects propagating normal to the sample surface[4,5].

Thickness gauging typically uses reflections of bulk waves from the back face of the material[9,17]. In some samples the faces may not be parallel[1,18]; in this case, a wedge can be used to model the expected ultrasonic behaviour. With laser generation of ultrasound on metal samples the dominant mode generated is often a surface wave; however, longitudinal and shear waves are also generated, with a known directivity[19,20].

This paper considers the behaviour of these bulk waves and how they can be used for sample characterisation, such as measuring the angle of a defect or gauging the thickness of a sample with non-parallel faces. Firstly, the experimental techniques and modelling are described. Secondly, the arrival times of the reflected and mode converted waves are calculated. Finally, we consider the variation in wave amplitude with scan position for several wavemodes, and calculate this using knowledge of the directivity of the generated signals and the changes in amplitude of the waves on reflection at the back and front faces

of the wedge.

The behaviour of the wave propagation in aluminium samples has been studied using experiments and finite element method (FEM) models, for laser generation and detection of ultrasound. The longitudinal and shear waves generated in the thermoelastic (low power) regime, chosen so that limited-to-no damage was done to the sample, have amplitudes which vary with propagation direction. These amplitudes are given by

$$u_L(\beta) \propto \frac{\sin(2\beta) \times (k^2 - \cos^2\beta)^{\frac{1}{2}}}{(k^2 - 2\cos^2\beta)^2 + 4\cos^2\beta(1 - \cos^2\beta)^{\frac{1}{2}}(k^2 - \cos^2\beta)^{\frac{1}{2}}} \tag{1}$$

for the longitudinal wave, where k is a normalised wavenumber defined by $k = c_L/c_S$, and $c_L = 6300$ m/s and $c_S = 3110$ m/s are the longitudinal and shear wave velocities in aluminium, and

$$u_S(\beta) \propto \frac{-k \sin 4\beta}{k(1 - 2\cos^2\beta)^2 + 4\cos^2\beta(1 - \cos^2\beta)^{\frac{1}{2}}(1 - k^2\cos^2\beta)^{\frac{1}{2}}} \tag{2}$$

for the shear wave (adapted from references[19–21] for this geometry). The angle β describes the propagation angle of the ultrasonic wave, and is labelled in the inset to figure 1.

Experiments used a 1064 nm Nd:YAG laser with a rise-time of 10 ns, focussed into a line source of approximate dimensions 6×0.5 mm[13,19,21]. Detection of the ultrasound was done using an IOS two-wave mixer interferometer, allowing a direct measurement of the out-of-plane displacement of the material surface with no surface preparation required[22]. The wedge sample was made from aluminium, of approximate dimensions 100 mm wide x 136 mm long with a wedge apex angle of 10°. The generation laser was held fixed while the detection laser was scanned towards the wedge tip, with the experimental set-up shown in the inset to figure 1.

The behaviour in a 10° aluminium wedge was also modelled using PZFlex, a FEM program, with absorbing boundaries used for all side faces to reduce reflections, and the generation laser modelled as a dipole force[13]. Both the in-plane and out-of-plane surface displacements were calculated and figure 1 shows typical A-Scans for two generation-detection separations. The large feature labelled R is the broadband Rayleigh wave; however, a large number of other wave-modes are also visible.

Figure 2 shows the modelled out-of-plane surface displacement for a fixed laser generation point with the detection point scanned towards the wedge tip, for a 10° aluminium wedge, presented as a B-Scan. At each detection position an A-Scan has been recorded and these are

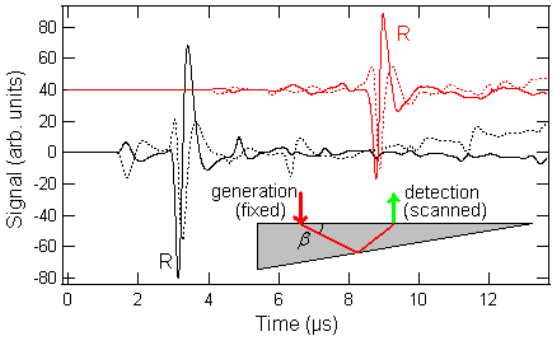

FIG. 1. FEM: A-Scans at two generator-detector separations (8.6 mm (lower) and 25 mm (upper)) on a 10° wedge. Solid lines show in-plane surface displacement, dotted lines the out-of-plane.

stacked to form the image, with the colour showing the amplitude. The behaviour in the B-Scan splits approximately into two regimes; in the top section of the figure, close to the wedge tip, the incident wavemodes experience a sample which has a reducing frequency·thickness product, and hence the wavemodes propagate as guided waves[5]. However, far from the tip (lower part of figure 2) the waves can be treated as Rayleigh, longitudinal, or shear modes. The Rayleigh wave has an arrival time which is linear with increasing separation of the generation and detection lasers, whereas the longitudinal and shear wavemodes, which have been reflected at the back face of the wedge and detected after one or more reflections and/or mode-conversions, have a more complicated dependence on scan position due to the variation in the path length for each mode as the laser separation is increased.

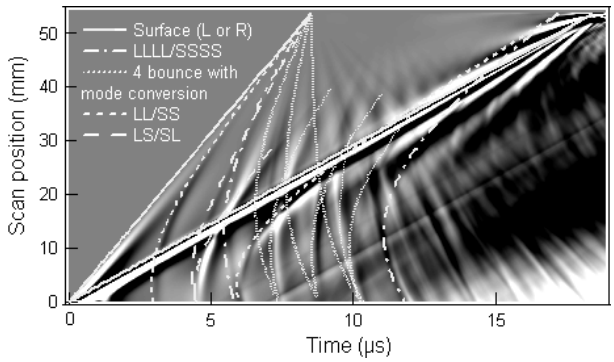

FIG. 2. FEM: B-Scan for a 10° wedge with wave arrival times overlaid, showing the out-of-plane surface displacements.

The arrival times of the longitudinal and shear waves can be calculated, giving a measure of the dimensions and angle of the wedge, and these are shown as lines on figure 2 and ex-

plained below. We consider the propagation times of the different wave modes (longitudinal, L; shear, S; multiple reflections and mode conversions, such as LL, SSSL etc.) for a given wedge angle.

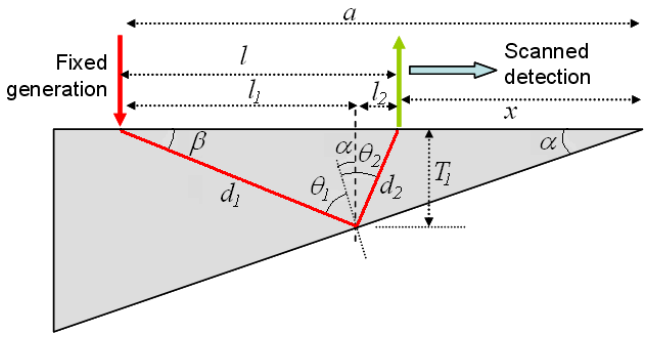

FIG. 3. Schematic for calculation of arrival time of waves. Multiple bounces can be calculated similarly.

Figure 3 shows a schematic for calculation of the arrival times for longitudinal and shear wavemodes which have been reflected once within the wedge, considering the LL, SS, LS or SL reflections. The distance a between the generation point and wedge tip for the model was 53.7 mm, while for the experiment a was 110 mm. α (the wedge apex angle) was 10°, and the direction of initial wave propagation, β, was varied from 0° to 90°, assuming generation in all directions.

From simple trigonometry it can be seen that the angle of incidence at the back face of the wedge is given by

$$\theta_1 = 90° - \alpha - \beta. \tag{3}$$

The angle of reflection is then given by

$$\theta_2 = \sin^{-1}\left[\frac{c_2}{c_1}\sin\theta_1\right], \tag{4}$$

where c_1 is the velocity of the incident wave and c_2 is the velocity of the reflected wave. The arrival position for each wave on the top surface, given an initial angle β, is $l = l_1 + l_2 = T_1\left[\tan(\theta_1 + \alpha) + \tan(\theta_2 - \alpha)\right]$, with all symbols defined in figure 3. By considering similar triangles, the thickness T_1 can be calculated as

$$T_1 = \frac{a\tan\alpha\tan\beta}{\tan\alpha + \tan\beta}. \tag{5}$$

The distance each wave travels is then a combination of known quantities, with

$$d_1 = \frac{T_1}{\cos(\theta_1 + \alpha)} \qquad \& \qquad d_2 = \frac{T_1}{\cos(\theta_2 - \alpha)}. \tag{6}$$

Finally, the arrival time at a position l is given by

$$t = \sum_n \frac{d_n}{c_n}, \tag{7}$$

where n denotes the number of each step. One can similarly calculate the arrival times for surface waves and for multiple reflections of bulk wavemodes, allowing mode conversion on each reflection, giving modes such as LLLL and LLSL.

Figure 2 shows the B-Scan of the modelled results, with the calculated wave arrival times overlaid, showing excellent agreement with the model results. A selection of multiple-bounce wavemodes have been presented; the exact arrival time depends on the order of the mode-conversion, e.g. LLLS or LSLL. Figure 4 shows experimental measurements on the top face of an aluminium wedge, with the arrival times calculated using equations 3 to 7 shown for selected wavemodes. Again, excellent agreement is shown between the calculated and measured arrival times.

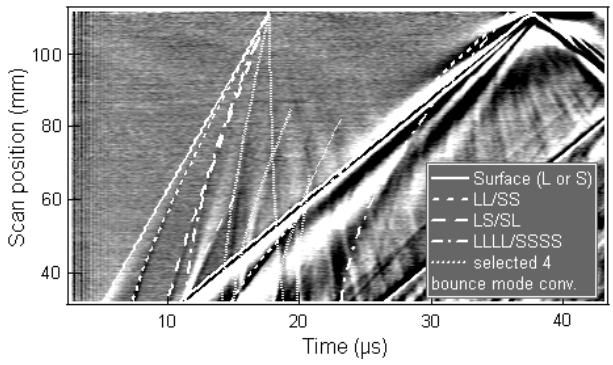

FIG. 4. Experiment: B-Scan for a 10° wedge with wave arrival times overlaid, showing the out-of-plane surface displacements

Not all waves are equally prominent at each detection position, and there is a clear variation in amplitude with changing generation-detection separation. The detected amplitude of the waves will depend on several factors. One must consider the attenuation of the wave during propagation, which will depend on the total distance travelled, $d = \sum d_n$. There will also be a dependence on the directivity of the generated waves[19,20], on the amplitude change

on reflection[19,23,24], and on the proportion of the motion in the out-of-plane relative to the top surface of the wedge at the detection position.

The directivity of waves generated using laser ultrasound is given by equations 1 & 2. In equations 3 to 7 it has been assumed that all values of β are equally likely; equations 1 & 2 can be used to calculate the amplitude of the longitudinal and shear waves which are generated as a function of propagation angle. The change in amplitude on reflection and mode-conversion has been described previously for a simple parallel-face block[19,24]. A longitudinal wave incident on the back face of the wedge, with incident angle θ_1, can be reflected either as a longitudinal wave or as a shear wave with angle θ_2 given by equation 4, and similarly for an incident shear wave. To calculate the amplitude following reflection, θ_2 for the mode-converted wave must be known, and is labelled γ in the following equations. For an incident longitudinal wave of amplitude $u_L(\beta)$ the resulting reflected wave from the back face of a wedge will have amplitude

$$A_L(\beta) = u_L(\beta)\frac{\sin 2\theta_1 \sin 2\gamma - k^2 \cos^2 2\gamma}{\sin 2\theta_1 \sin 2\gamma + k^2 \cos^2 2\gamma}$$
$$A_S(\beta) = u_L(\beta)\frac{2k \sin 2\theta_1 \cos 2\gamma}{\sin 2\theta_1 \sin 2\gamma + k^2 \cos^2 2\gamma} \tag{8}$$

for the reflected longitudinal and shear waves respectively. For an incident shear wave of amplitude $u_S(\beta)$ the reflected waves will have amplitudes

$$B_L(\beta) = u_S(\beta)\frac{-k \sin 4\theta_1}{\sin 2\theta_1 \sin 2\gamma + k^2 \cos^2 2\theta_1}$$
$$B_S(\beta) = u_S(\beta)\frac{\sin 2\theta_1 \sin 2\gamma - k^2 \cos^2 2\theta_1}{\sin 2\theta_1 \sin 2\gamma + k^2 \cos^2 2\theta_1}. \tag{9}$$

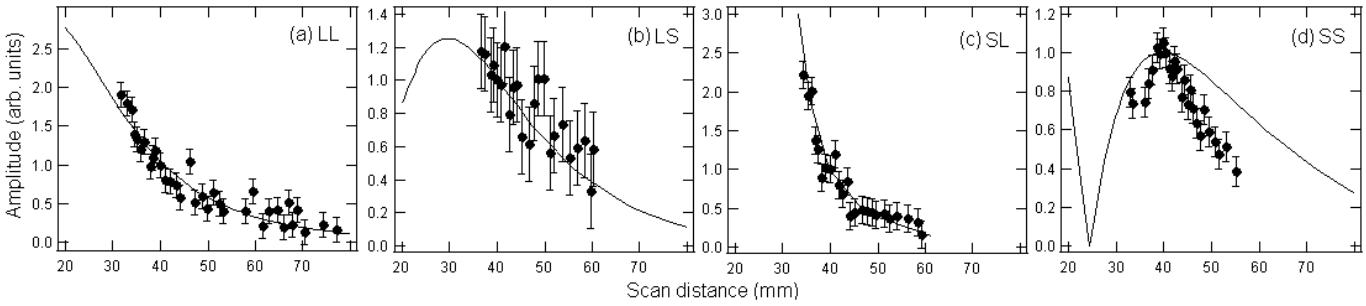

FIG. 5. The calculated (lines) and measured (points) wave amplitudes, normalised at a scan distance of 40 mm, for LL, LS, SL and SS.

The proportion of the wave motion in either the in-plane or out-of-plane relative to the top surface will depend on whether the wave is longitudinal or shear, and on the direction

of propagation relative to the sample surface on detection. For example, at very short detection distances (large β) the longitudinal wave will hit the sample surface approximately normally, hence will be predominantly out-of-plane when detected, whereas the shear wave will be predominantly in-plane. For long detection distances (small β) the wave is close to surface skimming, and hence the longitudinal wave has predominantly in-plane displacement. Considering this with the attenuation for a total travel distance of d, and the angle of incidence relative to the surface $\theta_I = 100^\circ - \theta_2$, the following amplitudes are predicted;

$$\begin{aligned} LL: &\quad A_L(\beta)\sin(\theta_I)/d \\ LS: &\quad A_S(\beta)\cos(\theta_I)/d \\ SL: &\quad B_L(\beta)\sin(\theta_I)/d \\ SS: &\quad B_S(\beta)\cos(\theta_I)/d. \end{aligned} \tag{10}$$

Figure 5 shows the solution of these equations for four modes as a function of separation of the generation and detection laser points, plotted as lines, normalised to 1 at a separation of 40 mm to account for the proportionality constant in equations 1 & 2. Shown as points are the normalised experimental wave amplitudes taken from the data in figure 4, with errors calculated by considering the variation in amplitude due to noise. For LL, LS and SL the amplitudes show excellent agreement, with the calculations predicting the change in amplitude with scan distance, confirming the validity of the measurement technique. For the SS wave poor agreement is seen. However, as can be seen on figure 4 this wave coincides with several other wavemodes, in particular the large amplitude Rayleigh wave, and hence an accurate measure of the amplitude is extremely difficult. For waves which do not interfere significantly with other wavemodes, the amplitude variation as a function of generation and detection separation can be used to characterise the sample geometry.

Recent work has shown that a wedge can be used as a model of an infinite depth angled defect, as an ocean wedge, or as a sample with varying thickness. Laser generated longitudinal and shear modes can also be used to characterise the wedge angle, based on knowledge of the wave velocities and the separation of the generation and detection points. The arrival times of the reflected and mode-converted waves depend on the wedge angle. Furthermore, the amplitude of these waves can be understood by considering the directivity of the generated waves, the change in amplitude on reflection and mode-conversion, the total distance of propagation and the component of the motion in the out-of-plane displacement

at the detector, and this again depends on the wedge geometry. This has the potential to lead to a new method of characterising the depth and angle of propagation of angled defects, plus a measure of the non-parallelicity of the front and back faces of a plate in thickness gauging.

This work was funded by the European Research Council under grant 202735, ERC Starting Independent Researcher Grant. We thank Professor Steve Dixon for help and advice with the research.

REFERENCES

[1]DK Hsu, AM Ayres, M Guangda and M Guangwen, NDT&E International **27(2)** 75-82 (1994)

[2]VM Babich, VA Borovikov, LJ Fradkin, V Kamotski and BA Samokish, NDT & E International **37(2)** 105-109 (2004)

[3]JL Blackshire and S Sathish, Appl. Phys. Lett. **80(18)** 3442-3444 (2002)

[4]B Dutton, AR Clough and RS Edwards, J. Nondestruct. Eval. **30(2)** 64-70 (2011)

[5]RS Edwards, B Dutton, AR Clough and MH Rosli, Appl. Phys. Lett. **99(9)** 094104 (2011)

[6]K Fujii, S Takeuchi, Y Okano and M Nakano, B. Seismol. Soc. Am. **74(1)** 41-60 (1984)

[7]Z Alterman and R Nathaniel, B. Seismol. Soc. Am. **65(6)** 1697-1719 (1975)

[8]JK Cooper, DC Lawton and GF Margrave, Geophysics **75(2)** T15-T21 (2010)

[9]DF Cannon, K-O Edel, SL Grassie and K Sawley, Fatigue Fract. Engng. Mater. Struct. **26** 865 (2003)

[10]J Jia, ZH Shen, LJ Wang and L Yuan, Chinese Optics Letters **9(2)** 022501 (2011)

[11]CH Yang and KY Tsai, Japanese Journal of Applied Physics (Part I) **43(7A)** 4392-4393 (2004)

[12]X Jia and M de Billy, Appl. Phys. Lett. **61(25)** 2970-2972 (1992)

[13]B Dutton, AR Clough, MH Rosli and RS Edwards, NDT&E International **44(4)** 353-360 (2011)

[14]KhB Tolipov, J. Appl. Mech. Tech. Phy. **51(1)** 22-30 (2010)

[15]BV Budaev and DB Bogy, Wave Motion **22** 239-257 (1995)

[16]X Jian, S Dixon, N Guo and RS Edwards, J. Appl. Phys. **101(6)** 064906 (2007)

[17]J Blitz and G Simpson, *Ultrasonic methods of non-destructive testing* (1996) Chapman & Hall, London

[18]CM Dao, S Das, S Banerjee and T Kundu, International Journal of Solids & Structures **46(11-12)** 2486-2492 (2009)

[19]CB Scruby and LE Drain, *Laser Ultrasonics: techniques and applications* (1990) Adam Hilger, Bristol

[20]DA Hutchins, RJ Dewhurst and SB Palmer, J. Acoust. Soc. Am. **70(5)** 1362-1369 (1981)

[21]AM Aindow, RJ Dewhurst and SB Palmer, Optics Communications **42(2)** 116-120 (1982)

[22]MB Klein, GD Bacher, A Grunnet-Jepsen, D Wright and WE Moerner, Optics Communications **162** 79-84 (1999)

[23]D Knauss and GAD Briggs, J. Phys. D: Appl. Phys. **27(9)** 1976-1983 (1994)

[24]JD Achenbach, *Wave propagation in elastic solids* (1973) North-Holland Pub. Co., Amsterdam